Hydrogeology Journal (2013) 21: 1731–1747
DOI 10.1007/s10040-013-1037-5

Indicator geostatistics for reconstructing Baton Rouge aquifer-fault hydrostratigraphy, Louisiana, USA

Ahmed S. Elshall · Frank T.-C. Tsai · Jeffrey S. Hanor

Abstract The complex siliciclastic aquifer system underneath the Baton Rouge area, Louisiana (USA), is fluvial in origin and is characterized by strongly binary heterogeneity of sand units and mudstones as pervious and impervious hydrofacies. The east–west trending Baton Rouge fault and Denham Springs-Scotlandville fault cut across East Baton Rouge Parish and play an important role in groundwater flow and aquifer salinization. This study reconstructs the Baton Rouge aquifer-fault system architecture for a Miocene-Pliocene depth interval that consists of the 1,200-foot sand to the 2,000-foot sand. The results show the spatial extent of sand units, their interconnections, and flow paths within each sand unit. The regional-scale formation dip, the sand unit offset on the faults, and the volumetric spatial extent of individual sand units are quantified. The study reveals the complexity of the Baton Rouge aquifer-fault system where the sand deposition is non-uniform, different sand units are interconnected, the sand unit displacement on the faults is significant, and the spatial distribution of flow pathways through the faults is sporadic. The identified locations of flow pathways through the Baton Rouge fault provide useful information on possible windows for saltwater intrusion from the south.

Keywords Aquifer characterization · Geostatistics · Hydrostratigraphy · Fault architecture · USA

Received: 14 December 2012 / Accepted: 6 August 2013
Published online: 2 October 2013

A. S. Elshall · F. T.-C. Tsai (✉)
Department of Civil and Environmental Engineering,
Louisiana State University, 3418G Patrick F. Taylor Hall,
Baton Rouge, 70803, USA
e-mail: ftsai@lsu.edu
Tel.: +1-225-5784246

A. S. Elshall
e-mail: aelsha1@lsu.edu

J. S. Hanor
Department of Geology and Geophysics,
Louisiana State University, 211 Howe-Russell Building,
Baton Rouge, 70803, USA
e-mail: hanor@lsu.edu

Introduction

The Baton Rouge aquifer system in southeastern Louisiana, USA, is part of the Southern Hills regional aquifer system (Buono 1983) and is a siliciclastic aquifer system consisting of a complexly interbedded series of fluvial sand and clay units (Chamberlain 2012) that thicken and dip southward (Tomaszewski 1996). This sequence of aquifers/aquitards extends to a depth of 3,000 feet (914.4 m) in the Baton Rouge area. According to Chamberlain (2012) the vertical alternation of sand-dominated units and clay-dominated units reflects cyclic variations in sea-level, with amalgamated fluvial sand bodies having been generally deposited during sea-level lowstands and mudstones during transgressive highstands. The sand units have variable thicknesses ranging from 20–300 feet (6.10–91.44 m). The study area shown in Fig. 1 focuses on late Miocene-Pliocene deposits of the 1,200-foot sand, the 1,500-foot sand, the 1,700-foot sand and the 2,000-foot sand. These sand units were classified and named by their approximate depth below ground level in Baton Rouge industrial district (Meyer and Turcan 1955). The Baton Rouge fault system, which consists of the Baton Rouge fault and the Denham Springs-Scotlandville fault (Tepetate fault), is an east–west trending fault system that crosscuts this aquifer/aquitard sequence (McCulloh and Heinrich 2012). The low permeability of the Baton Rouge fault historically separates the sequence of freshwater and brackish aquifers immediately north and south of the fault, respectively. The natural direction of water flow in the aquifer system is southward. However, heavy public supply and industrial groundwater pumping reversed the flow direction near the Baton Rouge fault and has resulted in saltwater encroachment across the fault (Rollo 1969; Tomaszewski 1996). To better understand salinization underneath Baton Rouge and the role of the geological faults as conduits and barriers (Bense and Person 2006; Hanor et al. 2011) to fluid flow, it is imperative to study the detailed hydrostratigraphic architecture of the Baton Rogue aquifer-fault system.

Constructing hydrostratigraphic architecture depends on the type and density of hydrofacies data and the scale of heterogeneity characterization. Different scales include the sequence hydrostratigraphic scale (Miller et al. 2000; Scharling et al. 2009; Faunt et al. 2010), the hydrofacies assemblage scale (Weissmann et al. 1999; Trevisani and

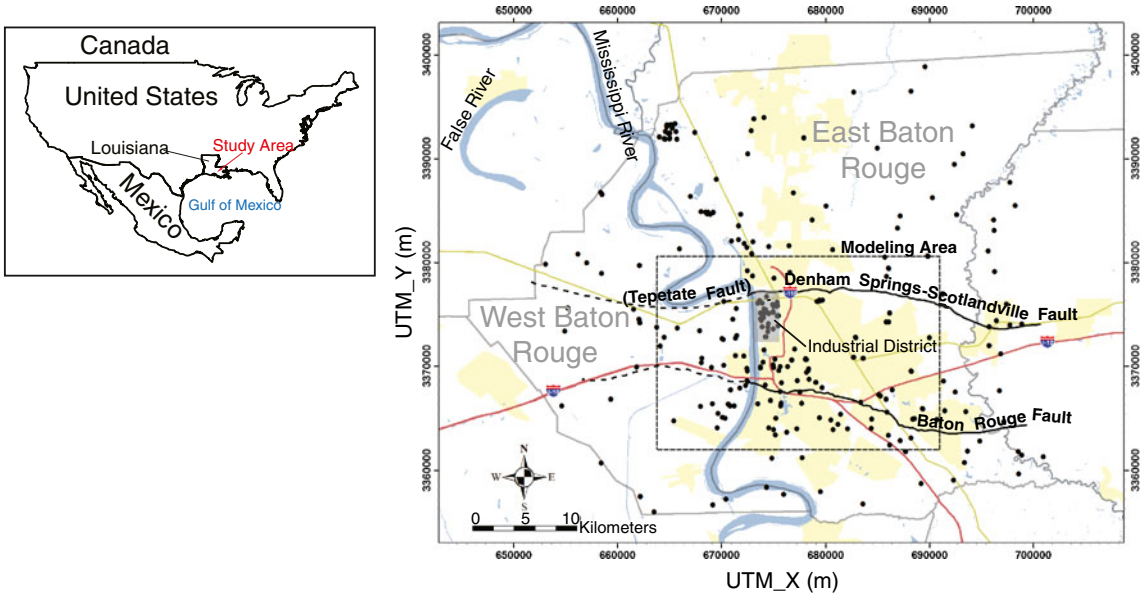

Fig. 1 Map of the study area in the Universal Transverse Mercator (UTM) coordinate system. *Black dots* represent the location of electric well logs. The *bold solid lines* are fault lines identified by the surface expression (McCulloh and Heinrich 2012). The *bold dashed lines* are the approximate surface locations of the faults (Griffith 2003). The *yellow areas* are urban areas, the *grey lines* are parish borders, the *red lines* are interstate freeways, the *green lines* are US highways, and the *blue areas* and lines are water bodies

Fabbri 2010), the hydrofacies unit scale (Zappa et al. 2006; Engdahl et al. 2010) and combinations of different heterogeneity scales (Weissmann and Fogg 1999; Proce et al. 2004; Comunian et al. 2011). This study focuses on the sequence hydrostratigraphic scale to obtain a detailed distribution of the thickness, lateral extent and depth of sand units underneath Baton Rouge. Following the classification of scales (Koltermann and Gorelick 1996), this scale is the same as the depositional environment scale, which is larger than the channel scale but smaller than the basin scale. This is also the same as the hydrofacies assemblages complex of Rubin (2003), which exhibits strong bimodal heterogeneity. A bimodal heterogeneity of pervious and impervious formations is conceptualized for the Baton Rouge aquifer system, in which sand assemblages complex and clay assemblages complex exhibit strong bimodal heterogeneity. For detailed descriptions of the depositional environmental scale of characterization and the concept of strong bimodal heterogeneity, the reader is referred to Rubin (2003, Figure 2.9).

The indicator geostatistics are particularly helpful in the Baton Rouge aquifer setting, since they are able to handle strongly bimodal heterogeneity. For the depositional environment scale of characterization, variogram-based geostatistics can still be a choice over the multiple-point training images geostatistics (Caers 2001; Strebelle 2002) when there are no predefined patterns of the shapes of the aquifer units in practice (Li et al. 2012a), as it is the case in this study area. Chamberlain (2012) interpreted these aquifer units as zones of amalgamated sand bodies that were created by fluvial aggradation following changes in sea levels and thus they are morphologically complex sand units with highly variable erosional unconformities. Since these sand units have irregular depositional and erosional patterns, indicator variogram-based geostatistics (Johnson and Dreiss 1989; Desbarats and Bachu 1994; Johnson 1995; Trevisani and Fabbri 2010) is used for indicator hydrostratigraphy modeling in this study. The indicator variograms as described by Journel (1983) are structurally informative (Johnson and Dreiss 1989). By empirically acknowledging the random and structured qualities of geological geometry, indicator variograms can depict sharp transitions in the spatial field (Johnson 1995).

This study employs the generalized parameterization method (Tsai and Yeh 2004; Tsai 2006) through an inversion scheme to obtain the hydrostratigraphic architecture. The generalized parameterization (GP) is a combination of indictor kriging (IK) and indicator zonation (IZ) for providing flexible nonsmooth conditional estimates. Indicator zonation divides the space into a number of non-overlapping zones based on an indicator function and provides sharp-edged estimations (e.g. Tsai 2009). On the other hand, indictor kriging provides smooth estimations. Since boundaries between sand and clay units are neither smooth, nor blocky as a result of fluvial depositional processes, the GP is able to estimate the nonsmooth distribution of sand and clay units by combing both features of indicator kriging and indicator zonation through weighting coefficients. A second problem, which is peculiar to indicator geostatistics methods, is that the facies cutoff that rounds the model estimates into binary values to produce the indicators is unknown. To simplify this problem previous studies (Johnson and Dreiss 1989; Falivene et al. 2007) have considered a cutoff value of 0.5 as a reasonable assumption. Yet fixed cutoff value 0.5 results in an underestimation of the facies that exists in less proportion. Thus, this unknown model

 DOI 10.1007/s10040-013-1037-5

parameter needs to be calibrated. Thirdly, to calculate the structure of the experimental variogram, it is important to establish correct correlations among well logs to account for the spatial continuity of the deposits. Different formation dips have a significant effect on the selection of data points and the variogram structure, and thus the formation dip is considered as an unknown model parameter. Estimating the weighting coefficients of the GP method along with two other unknown model parameters, which are the cutoff and the formation dip, through an inversion scheme, addresses these three aforesaid issues of the variogram-based geostatistics.

Several studies have utilized abundant hydrofacies data to reconstruct sedimentary architecture from geophysical logs and lithologic logs. This includes the use of electrical resistivity data (Schulmeister et al. 2003; Tartakovsky et al. 2008), multiple geophysical data types (Linde et al. 2006; Wiederhold et al. 2008), and combined geophysical data and lithologic data (Ezzedine et al. 1999; Chen and Rubin 2003; Bersezio et al. 2007). This study uses binary sand and clay hydrofacies data from electric well logs for reconstructing images of the subsurface and lithologic data from drillers' logs as the calibration data.

Using this scheme to reconstruct the hydrostratigraphic architecture, this study will provide essential information on the Baton Rouge aquifer-fault system, which has never been studied in such detail in the past. The resulting hydrostratigraphic architecture will provide a detailed distribution of the thickness, lateral extent and depth of different sand units. The formation dip, sand offset on the faults, and volumetric sand proportion can be quantified. The hydrostratigraphic architecture will also improve the understanding of potential interconnections among different sand units resulting from the complexity of fluvial deposition. Most importantly, the study will provide essential information on the flow pathways across the Baton Rouge fault and the Denham Springs-Scotlandville fault. Figure 1 shows the location of the faults, which have a significant role on groundwater flow to water wells in the Baton Rouge metropolitan area and industrial district. Mapping the architecture of the two faults has never been done before and is of particular importance since the public supply in the Greater Baton Rouge area is 100 % dependent on groundwater, and local industries use groundwater as much as the public supply (Sargent 2012). In addition, the result will provide essential information on identifying potential flow pathways through the Baton Rouge fault with regard to saltwater encroachment.

The outline of the report is as follows. The proposed geological architecture model is first described. This includes the model data, the generalized parameterization method and an inversion scheme to estimate the unknown model parameters. This is followed by presenting the inverse results with a brief illustration of the main features of the generalized parameterization method with respect to indicator kriging and indicator zonation. Then the hydrogeological findings of the Baton Rouge aquifer-fault system are presented and discussed.

Model data

Electric and drillers' well log data that are used in this study are from elevations of –1,000 ft (–304.8 m) to –3,000 ft (–914.4 m) NGVD29. The vertical discretization is at 1-foot (0.304 m) intervals.

For geostatistical reconstruction of subsurface formation, the study uses 288 electric well logs with 237 water well logs and 51 oil/gas well logs. The sand-clay sequence interpretation for each log is based on electrical resistivity, spontaneous potential (SP), and gamma ray. In general, shallow electrical resistivity (e.g., short-normal resistivity, medium induction resistivity, etc.) of 20 ohm-m is a good threshold for water-well logs to identify sand units for the freshwater formations in southeastern Louisiana. When salty water is present instead, the spontaneous-potential response helps to identify sand units. When available, the gamma ray response is used as a guide along with resistivity and spontaneous potential to identify sand units. For example, in Fig. 2 the saline sands are identified in well log EB-783 located at the south of the Baton Rouge fault using SP and resistivity. For a saline sand, the SP response is pronounced and the long normal resistivity is less than the short normal resistivity. Also, the presence of salt water can be seen at the bottom of the sand in the depth of 2,200 feet. Freshwater sands are identified in well log EB-1317 (south of the Baton Rouge fault) and WBR-128 (south of the Baton Rouge fault) based on resistivity. SP is not pronounced in these two well logs. Low gamma ray in EB-1317 correlates sand units.

While inverse modeling is generally utilized for hydrofacies reconstruction by conditioning on piezometric head or on concentration data (e.g. Zhou et al. 2012; Li et al. 2012b), this study uses lithologic data from drillers' logs as the calibration data. For model calibration lithologic data from 93 drillers' logs are used. For each well log, lithologic data represents the actual lithology with depth. Interpreting drillers' logs can be subjective and thus assigning binary indicator values to the drillers' logs is uncertain. To achieve a consistent interpretation of drillers' logs, lithologic descriptions are categorized into three categories: sand facies, clay facies and undetermined facies as listed in Table 1.

To achieve consistency with the electric-well log interpretation, sand and gravel are considered to belong to the sand facies indicator 1 and other materials belong to the clay facies indicator 0. This point is illustrated in Fig. 2, which shows lithology columns where both the drillers' logs and electric logs are available. For observation well WBR-128, drillers' terms such as "sand", "sand: fine, medium, gray" and "sand: fine, gray" are easily interpreted as sand facies indicator 1. Similarly, terms such as "shale", "shale: blue, gray, sandy" are easily interpreted as clay facies indicator 0. Indistinct terms such as "shale, sand, and silt streaks" are interpreted as clay facies indicator 0. Similarly, for observation well EB-1317 the indistinct term "shale with sand streaks" is interpreted as clay facies indicator 0. This is to maintain consistency with the electric logs interpretation in which distinct sand only is assigned sand facies indicator 1. For the well logs EB-1317 and WBR-128 in Fig. 2, the interpretation of the drillers' log shows very good match

 DOI 10.1007/s10040-013-1037-5

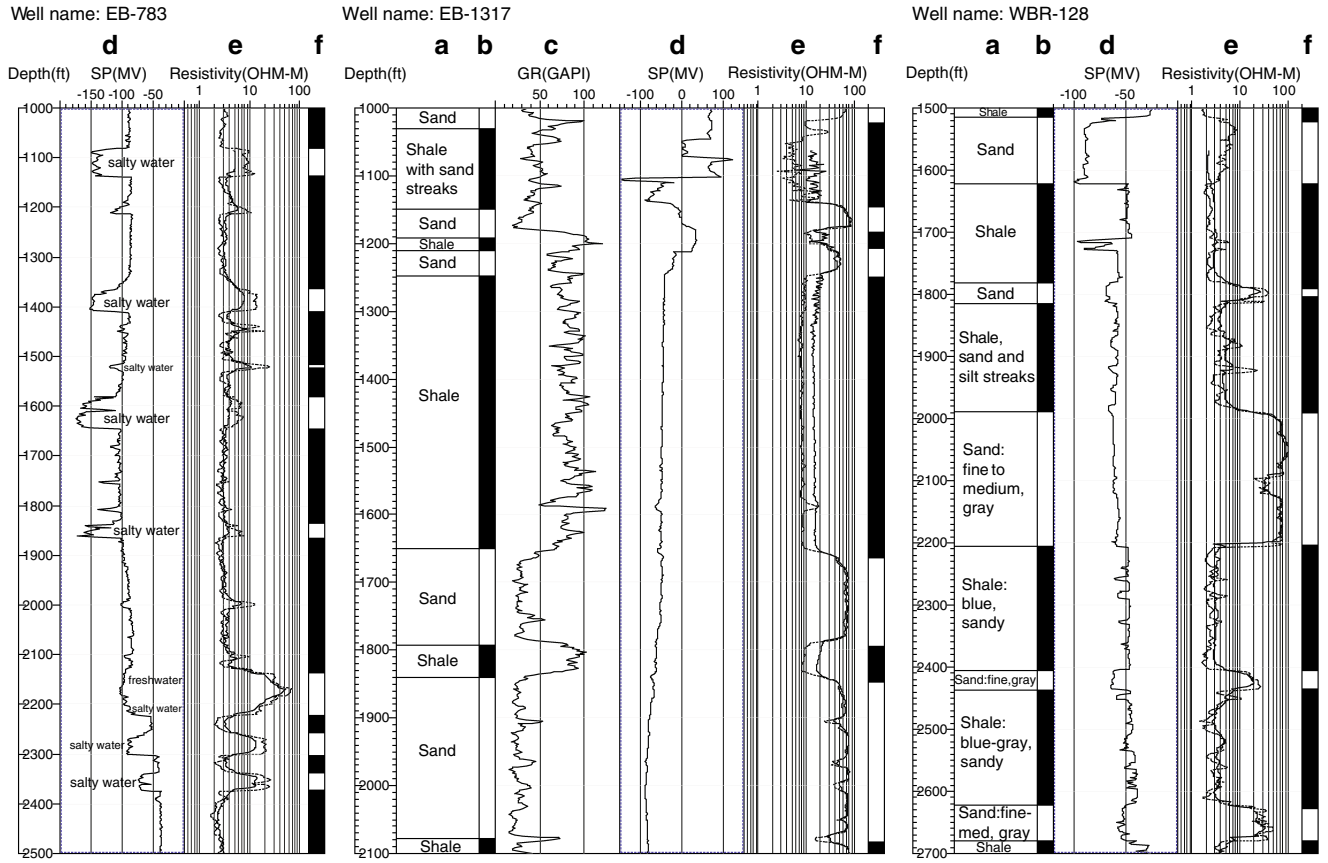

Fig. 2 Wells logs for water well *EB-1317*, north of the Baton Rouge fault, and water wells *EB-783* and *WRB-128*, south of the Baton Rouge fault. Column index is as follows: (*a*) drillers' log, (*b*) binary interpretation of drillers' log (*white* for sand and *black* for clay), (*c*) gamma ray (GR), (*d*) sponteneous potential (SP), (*e*) short normal resistivity (*dotted line*) and long normal resistivity (*solid line*), and (*f*) binary interpretation of electric log (*white* for sand and *black* for clay)

with the interpretation of the electric logs. The mismatch of the interpreted indicators from the drillers' log and the electric logs is 3.0 % for WBR-128 and 4.6 % for EB-1317. The average mismatch for the 19 well logs in the used data set where both drillers' logs and electric logs are available is 7.12±2.44 %. This indicates that the selected 93 drillers' logs tend to have adequate quality and that the interpretation and the indicator assignment for the drillers' logs and electric logs are consistent.

Modeling area

Different fault characterizations can lead to different model structures (Chester et al. 1993; Bredehoeft 1997; Salve and Oldenburg 2001; Fairley et al. 2003; Nishikawa et al. 2009). The Baton Rouge fault system is composed of the Baton Rouge fault and the Denham Springs-Scotlandville fault. The Baton Rouge fault is listric growth fault (McCulloh and Heinrich 2012) that crosscuts the aquifer units causing the aquifers to be offset up to 344 ft (105 m) at the top of the 2,000-foot sand (Durham and Peeples 1956). Little is known about the Denham Springs-Scotlandville fault, and the displacement of the aquifer units on this fault is not well characterized. Rollo's (1969) hydrofacies mapping of the Baton Rouge aquifer system did not recognize the presence of the Denham Springs-Scotlandville fault, and thus the aquifer units north of the Baton Rouge fault appear continuous on Rollo's (1969) cross sections.

Table 1 Interpretation of drillers' logs into three lithological facies and indicator assignment

Facies	Sand	Undetermined	Clay
Lithologic description	Sand: fine, packed, very fine, good, medium, coarse, loose, yellow, hard packed, packed, pay, sandstone, gray, lightly gray, tight, with shell fragments, with wood, gray-white, blue-gray, with gravel	Clay and sand, shale and sand, streaks of sand and shale, shaly sand, poor sand and streaks of shale, sand and hard sandy shale	Clay: blue, hard, soft, gray green, brown, dark brown highly organic, tan, red-brown, green, with sand strings Shale: heavy, sandy, hard, red, brown, sticky, yellow, with mixed gravel, with streaks of sand, with some sand breaks
Indicator	1	0	0

DOI 10.1007/s10040-013-1037-5

By recognizing the presence of the Denham Springs-Scotlandville fault, the modeling area in Fig. 1 results in three geographic modeling domains: a domain south of the Baton Rouge fault, a middle domain between the Baton Rouge fault and the Denham Springs-Scotlandville fault, and a domain north of the Denham Springs-Scotlandville fault. Aquifer architectures are independently reconstructed for individual domains. The fault architecture is produced by juxtaposing the reconstructed aquifer architectures immediately north and south of the fault plane. For both the Baton Rouge fault and Denham Springs-Scotlandville fault, it is assumed that the fault planes are vertical, although deeper in the sections the faults are known to be dipping to the south (McCulloh and Heinrich 2012).

Indicator generalized parameterization for hydrostratigraphy modeling

In this study, parameterization is conducted in the 2D planar direction along the dip for every 1-foot vertical interval. Three-dimensional (3D) aquifer-fault architecture is reconstructed by assembling all two-dimensional slices.

This study utilizes a generalized parameterization (GP) method (Tsai and Yeh 2004; Tsai 2006), which combines the indicator kriging (IK) and indicator zonation (IZ) through a set of data weighting coefficients to obtain nonsmooth conditional estimates. The indicator function $[I(\mathbf{x},v),\mathbf{x}\in\text{study area}]$ is a random function with the indicator random variable v describing the spatial extent of sand or clay facies. For a given sand-clay cutoff α, the random function of the indicator random variable v for sand facies is defined as

$$I(\mathbf{x},v)=\begin{cases}1 & v\in Sand,\ \ v(\mathbf{x})\geq\alpha\\ 0 & v\notin Sand,\ \ v(\mathbf{x})<\alpha\end{cases} \tag{1}$$

From Eq. (1) the indicator outcome (one or zero) indicates the presence of sand facies or clay facies, respectively. The indicator variogram has the same definition as the normal variogram except that the real random function is replaced by the indicator random function $I(\mathbf{x},v)$. To calculate the expected value $v^*(\mathbf{x}_0)$ at location x_0, the GP is

$$v^*(\mathbf{x}_0)=I(\mathbf{x}_\mathrm{k})+\sum_{i=1}^{N}\lambda_\mathrm{i}[I(\mathbf{x}_\mathrm{i})-I(\mathbf{x}_\mathrm{k})]\beta_\mathrm{i} \tag{2}$$

where N is the number of electric well logs, $I(\mathbf{x}_\mathrm{i})$ is the indicator data, λ_i is the indicator kriging weight, and β_i is the data weighting coefficient for a data point of a well log at location x_i. $I(\mathbf{x}_\mathrm{k})$ is indicator data for a zone defined by well log k. Equation (2) shows that GP estimate at unknown location is similar to IK estimate $v^*(\mathbf{x}_0)=\sum_{i=1}^{N}\lambda_\mathrm{i}I(\mathbf{x}_\mathrm{i})$ or the IZ estimate $v^*(\mathbf{x}_0)=I(\mathbf{x}_\mathrm{k})$ except for the introduction of β_i such that $\forall\beta_\mathrm{i}=1$ gives the IK estimate, $\forall\beta_\mathrm{i}=0$ gives the IZ estimate and $0<\beta_\mathrm{i}<1$ gives the in-between GP estimate. The indicator variance using the GP is

$$\alpha_v^2(\mathbf{x}_0)=\sum_{i=1}^{N}\sum_{j=1}^{N}\lambda_\mathrm{i}\lambda_\mathrm{j}R(\mathbf{x}_\mathrm{i},\mathbf{x}_\mathrm{j})\beta_\mathrm{i}\beta_\mathrm{j}-2\sum_{i=1}^{N}R(\mathbf{x}_\mathrm{i},\mathbf{x}_0)\beta_\mathrm{i}+2\gamma(\mathbf{x}_0,\mathbf{x}_\mathrm{k}) \tag{3}$$

where $R(\mathbf{x}_\mathrm{a},\mathbf{x}_\mathrm{b})=\gamma(\mathbf{x}_\mathrm{a},\mathbf{x}_\mathrm{k})+\gamma(\mathbf{x}_\mathrm{b},\mathbf{x}_\mathrm{k})-\gamma(\mathbf{x}_\mathrm{a},\mathbf{x}_\mathrm{b})$ and γ is the variogram. This study uses an exponential variogram model.

For zonal delineation, this study uses 2D Voronoi tessellation (Sibson 1980). This is a simple mathematical technique for dividing a space into a number of Voronoi zones, given a set of coplanar points, which are the electric well logs data. A Voronoi zone, which is drawn based on bi-sectors for each data point, is a boundary enclosing all the intermediate space lying nearest to that data point than to other data points in the plane. The Voronoi tessellation is considered a neutral and unbiased approach to define the neighborhood of a data point (Tsai and Yeh 2004; Tsai 2006).

Unknown model parameters

The first unknown model parameter is the formation dip, which establishes data correlation. The Baton Rouge aquifer system gently dips south. Prior geological studies did not quantify the formation dip. The dip was calculated to be 0.30°±0.06° from the USGS cross-sectional maps in the area (Griffith 2003) as prior information. To constrain the search space, the dip is set within the range $0.06°\leq\phi\leq0.60°$. The vertical tolerance of the dip is not reported in any study, and no vertical tolerance is considered.

The second unknown model parameter is the sand-clay cutoff value α. The estimated v values, which the cutoff value rounds to produce an indicator, could be viewed as the conditional probability with respect to the binary variables (Chilès and Delfiner 1999). The limits of the cutoff value α are constrained to a realistic but flexible range of $0.3\leq\alpha\leq0.7$.

Other unknown model parameters are the data weighting coefficients $\boldsymbol{\beta}$ of the well logs. The model used 288 geophysical well logs in which the south, middle and north domains have 61, 129 and 98 well logs, respectively, to reconstruct the hydrostratigraphy. When the spacing of well logs is dense, the estimates by the GP method in these areas become insensitive to the data weighting coefficients $\boldsymbol{\beta}$, since the indicator kriging estimates and indicator zonation estimates are similar. To reduce the computational cost of the inverse problem, insensitive values of $\boldsymbol{\beta}$ are identified through sensitivity analysis. Performing the sensitivity

 DOI 10.1007/s10040-013-1037-5

analysis starts by calibrating the hydrostratigraphy model only with respect to the dip and cutoff for given $\forall\beta_i$=1 to all well logs, and then using the calibrated model as a reference for the fitting error. Then taking one well log at a time, its data weighting coefficient is evaluated from 0 to 1 incrementally by 0.1 to calculate new fitting errors. Any well log that results in an error difference less than ±0.05 % from the calibrated model is considered to have a fixed data weighting coefficient β_i=1. The sensitivity analysis shows that 48 well logs have sensitive $\boldsymbol{\beta}$ coefficients with their number in the south, middle and north domains being 6, 34 and 8 well logs, respectively.

Inverse problem and calibration results

The data weighting coefficients $\boldsymbol{\beta}$ along with the dip ϕ and sand-clay cutoff α are the unknown model parameters to be estimated using an inversion scheme. The inversion scheme for the IZ, IK and GP is the same expect for the size of the unknown parameters. The IZ inversion has only one unknown parameter that is the dip. The unknown parameters of the IK inversion are the dip and the cutoff. The unknown parameters of the GP inversion are the dip, the cutoff and the data weighting coefficients. The inverse problem is formulated by minimizing the mean squared error between the estimated and observed facies as follows:

$$\min_{\phi,\alpha,\boldsymbol{\beta}} \quad \frac{1}{2}\left\{\frac{1}{M_{\text{sand}}}\sum_{i=1}^{M_{\text{sand}}}\left[I^{\text{i,est}}(\mathbf{x})-I^{\text{i,obs}}_{\text{sand}}(\mathbf{x})\right]^2+\frac{1}{M_{\text{clay}}}\sum_{i=1}^{M_{\text{clay}}}\left[I^{\text{i,est}}(\mathbf{x})-I^{\text{i,obs}}_{\text{clay}}(\mathbf{x})\right]^2\right\} \tag{4}$$

where M_{sand} and M_{clay} are the number of data points of the and facies and clay facies, respectively. The $I^{\text{i,est}}(\mathbf{x})$, $I^{\text{i,obs}}_{\text{sand}}(\mathbf{x})$ and $I^{\text{i,obs}}_{\text{clay}}(\mathbf{x})$ are the indicator estimate, the observed sand facies indicator and the observed clay facies indicator at a location $\mathbf{x}$, respectively. The mean squared error is separated into two error terms with one for each facies to avoid calibration bias toward favoring the fitting of clay over sand since the well logs indicate a clay proportion of about two-third by volume within the study area. The proportions of sand calculated from the electric logs and the drillers' logs are 0.338 and 0.339, respectively. Thus, this separation in Eq. (4) underlines that reducing the sand error is equally important as reducing the clay error.

To solve the inverse problem, the study adopts the covariance matrix adaptation evolution strategy (CMA-ES; Hansen et al. 2003) as a local derivative-free optimization algorithm for two reasons. First, unlike the derivative-based algorithms, using the CMA-ES allows for flexible optimization without prior assumptions or restrictions about the model structure. Second, the enhanced search properties of the CMA-ES allow for reaching near global solution. Similar to other generation-based optimization algorithms, the CMA-ES proposes several candidate solutions per search iteration. Each candidate solution is a vector of unknown model parameters, which the model uses to solve for the state variables. Then the objective functions of all solutions are calculated and ranked. The CMA-ES adapts a covariance matrix representing the pairwise dependency between unknown model parameters, which approximates the inverse of the Hessian matrix up to a certain factor. The covariance matrix adaptation uses information from the ranking of the current solutions and from the previous search path. Then the solutions are updated with the covariance matrix and an adaptable step size, which are adapted through two conjugates that implements heuristic control terms. These enhanced search properties allow the CMA-ES to handle ill-conditioned, nonsmooth, discontinuous, nonconvex and multimodal functions. Reviewing the CMA-ES algorithm is beyond the scope of this work, and reader is referred to Hansen (2006) and the references therein.

The inversion scheme steps are as follows. First, the CMA-ES generates candidate solutions, which are sets of unknown model parameters. Second, for each proposed solution the experimental variograms and a theoretical variogram are calculated based on the proposed dip. With respect to experimental variograms it is important to clarify that one precaution with respect to location dependence of data correlation is accounted for. The correlation between the data across the faults is prevented, but all the experimental variograms of each domain are grouped together to calculate one theoretical variogram. The theoretical variograms is fitted to the experimental variograms automatically through using the pattern search method of Hooke and Jeeves (1961). It performs direct directional search for the correlation parameters, which are the nugget, sill and effective range, to minimize the squared root error between the experimental and the theoretical variograms. Third, interpolation function in Eq. (2) is used to estimate facies distribution at unknown locations. For the inversion purpose the unknown locations are the drillers' logs locations. For the IZ inversion all the $\boldsymbol{\beta}$ values are set to zero, and thus the cutoff is not needed. Contrariwise, for the IK inversion the $\boldsymbol{\beta}$ values are set to one, thus the estimated facies is rounded to the indicator value by the cutoff. For the GP inversion $\boldsymbol{\beta}$ values are used by the interpolation function in Eq. (2) to estimate facies distribution at the unknown locations and the cutoff is used to round the indicator. Fourth, the estimated facies are compared to the observed facies using Eq. (4) to calculate the mean squared error for individual solutions. Then, step 1 is repeated until the mean squared error is minimized.

The outcome of the inversion is the best unknown model parameters set that fits the observed facies. This

 DOI 10.1007/s10040-013-1037-5

Table 2 Estimated variogram structural parameters and model parameters for the three methods

Method	Nugget	Sill	Range [m]	Dip [Deg.]	Cutoff	Sand proportion	Sand error[%]	Clay error[%]	Total error[%]
IZ	0.062	0.161	8,400	0.276	–	0.340	13.02	12.79	12.91
GP	0.083	0.139	8,400	0.289	0.404	0.347	11.96	12.90	12.43
IK	0.084	0.139	8,600	0.286	0.404	0.347	12.04	12.96	12.50

parameters set (dip, cutoff and β values) can be used to plot any 2D or 3D diagrams according to the desired grid size. For example, in this study all the cross sections of the faults have a grid size of 50 m along the fault lines. The 3D diagrams of the aquifer system have a grid size of 200 m in the X and Y directions. The discretization in Z direction is 1-foot (0.34-m) interval.

This inversion scheme is used to obtain the optimal data weighting coefficients, dip, and cutoff for the hydrostratigraphy model. The calibration results are shown in Table 2. The variogram structure and cutoff are similar for the indicator zonation (IK), generalized parameterization (GP), and indicator kriging (IZ) methods. The three methods also show the same dip around 0.29°and the same sand proportion around 0.35. The GP shows less fitting error than the IK and IZ methods due to the flexibility of the method.

To show the differences between the three methods, the architecture of the Denham Springs-Scotlandville fault and the Baton Rouge fault are used as examples. Figures 3 and 4 show the juxtaposition at the fault cross sections. Black areas are clay units north of the fault. Gray areas are clay units south of the fault. White areas show potential hydraulic connections formed by sand units from both sides of the fault. It is noted that the faults are 3D zones of deformation, not 2D planes. Determination of

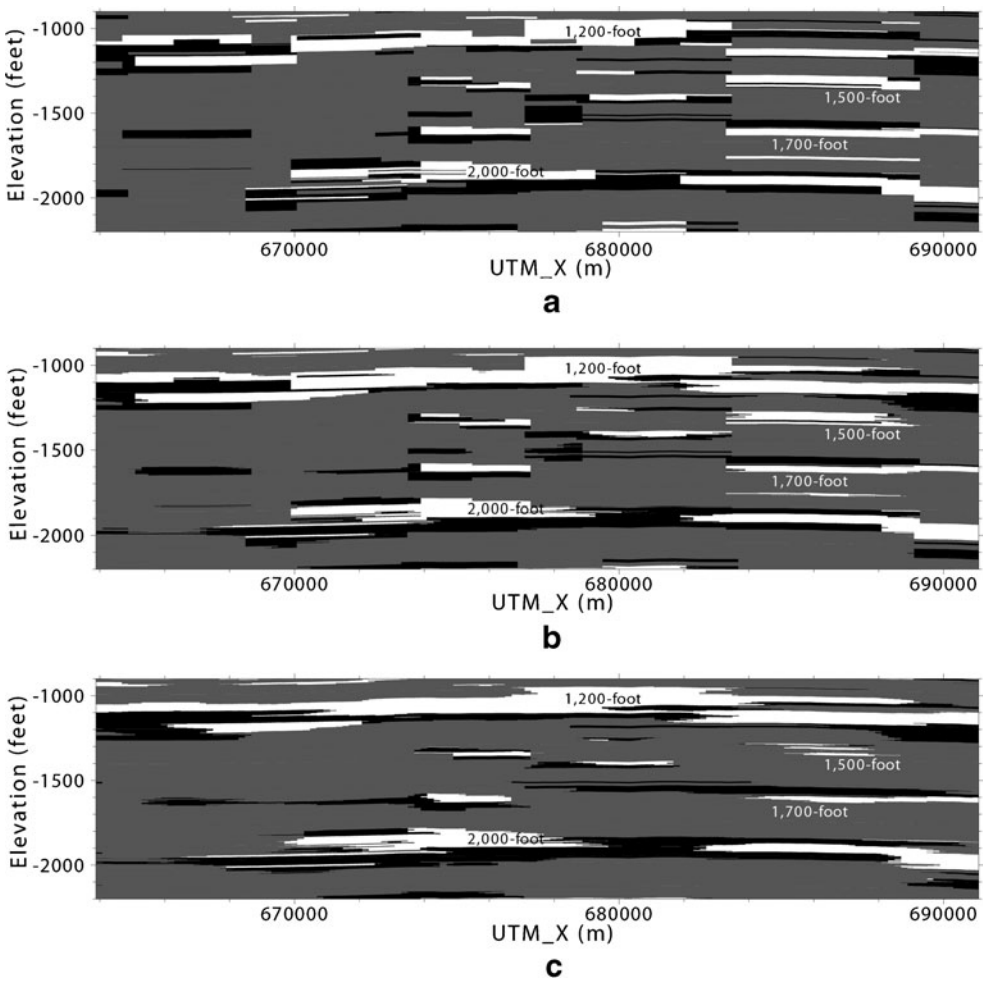

Fig. 3 The architecture of the Denham Springs-Scotlandville fault in the modeling area using **a** indicator zonation, **b** generalized parameterization, and **c** indicator kriging. *Black areas* are clay units north of the fault. *Gray areas* are clay units south of the fault. *White areas* show potential hydraulic connections formed by sand units from both sides of the fault. The fault cross sections are based on 3D estimates that follow the UTM_X and UTM_Y coordinates of the fault line in Fig. 1. Elevation is feet above NGVD29

 DOI 10.1007/s10040-013-1037-5

permeability of the fault zone is suggested by Bense and Person (2006) and Hanor et al. (2011). The detailed architecture of the fault zone is not the scope of this study. The three methods succeeded in capturing the main flow pathways through the faults. The facies shape using the GP estimate is neither as sharp-edged as the IZ estimate nor as smooth as the IK estimate, which is the main advantage of the GP method. The following results and discussion are based on the GP estimate.

Beside using three methods to understand the uncertainty of the estimates, the study further assesses the uncertainty of the unknown model parameters, which are the dip, cutoff and 48 β values. The CMA-ES provides the maximum likelihood estimate with a full covariance for the unknown model parameters. Hundred samples are obtained, which are random vectors each with the size of the unknown model parameters set chosen from the multivariate normal distribution with mean, and covariance. Figure 5 shows the results of the uncertainty analysis. Figure (5a,b) shows the realizations that have the minimum generated dip 0.23° and maximum generated dip 0.41° in all the realizations, respectively. It is important to note that for the steeper dip the flow pathway at the east in the 2,000-foot sand disappears. Figure (5c,d) shows the realizations that have the minimum generated cutoff 0.39 and maximum generated cutoff 0.42 in all the realizations, respectively. These two realizations have dips of 0.29° and 0.30°, respectively. Since these two figures are relatively similar, particularly with respect to main flow pathways across the fault, it can be concluded that the dip is the most sensitive parameter. Figure (5e–h) shows a randomly selected realization, ensemble average of the realizations, ensemble variance of the realizations at south of the fault and ensemble variance of the realizations at north of the fault, respectively. Again the emendable average (Fig. 5f) is comparable with the maximum likelihood estimate (Fig. 4b) with respect to the main flow pathways across the fault. However, it was unexpected to find the variance south of the fault (Fig. 5g) lower than the variance north of the fault, since is there are relatively fewer conditioning points to the south. However, this could be due to the distribution of the data points.

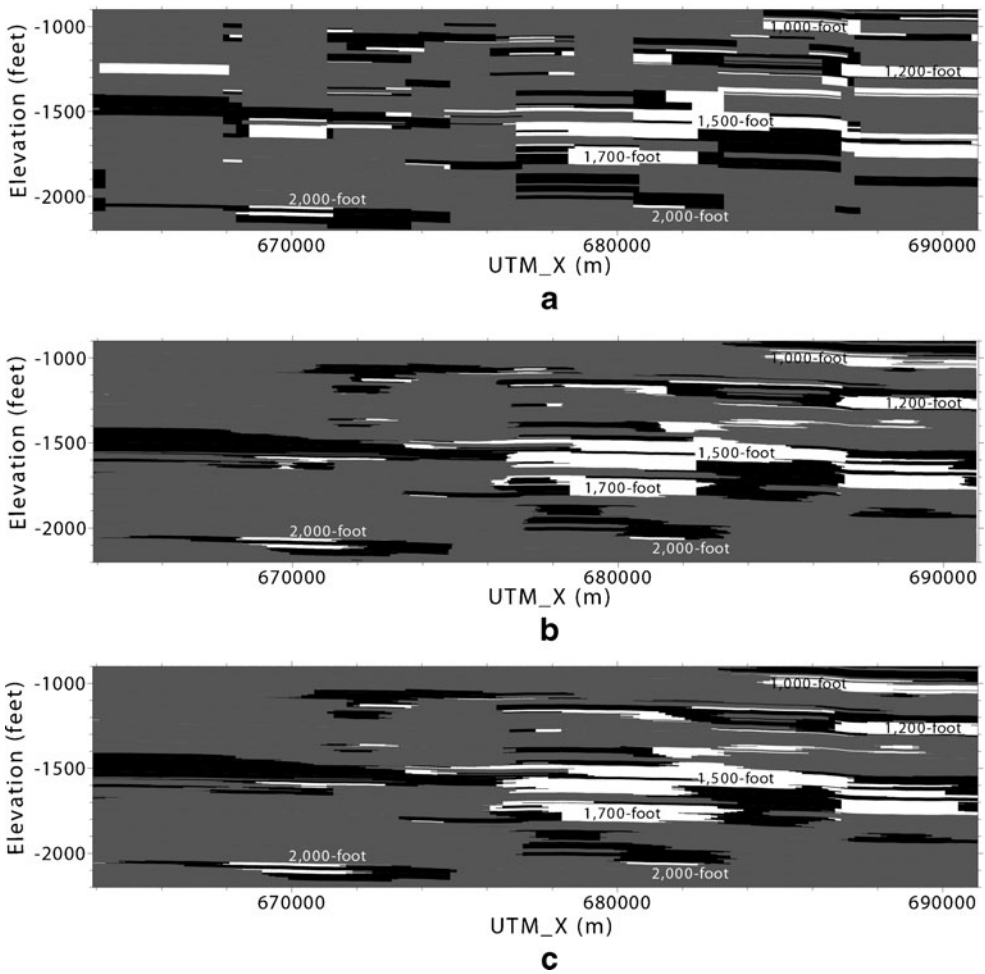

Fig. 4 The architecture of the Baton Rouge fault in the modeling area using **a** indicator zonation, **b** generalized parameterization, and **c** indicator kriging. *Black areas* are clay units north of the fault. *Gray areas* are clay units south of the fault. *White areas* show potential hydraulic connections formed by sand units from both sides of the fault. The fault cross sections are based on 3D estimates that follow the UTM_X and UTM_Y coordinates of the fault line in Fig. 1

 DOI 10.1007/s10040-013-1037-5

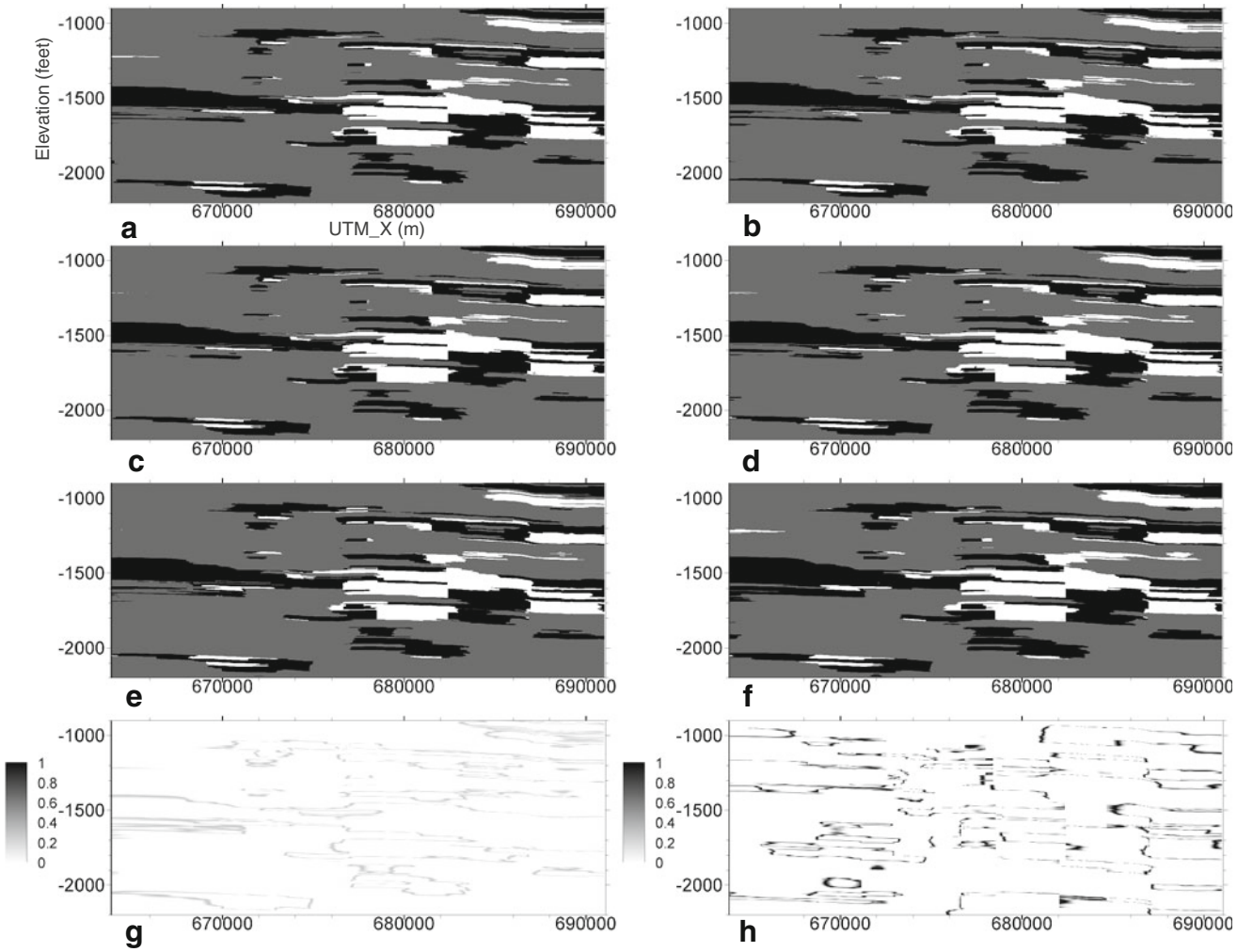

Fig. 5 The architecture of the Baton Rouge fault in the modeling area (see Fig. 1): **a**–**e** different realizations, **f** ensemble average of 100 realizations, **g** ensemble variance of 100 realizations for south of the fault, **h** ensemble variance of 100 realizations for north of the fault. *Black areas* in **a**–**f** are clay units north of the fault. *Gray areas* are clay units south of the fault. *White areas* show potential hydraulic connections formed by sand units from both sides of the fault. The fault cross sections are based on 3D estimates that follow the UTM_X and UTM_Y coordinates of the fault line in Fig. 1

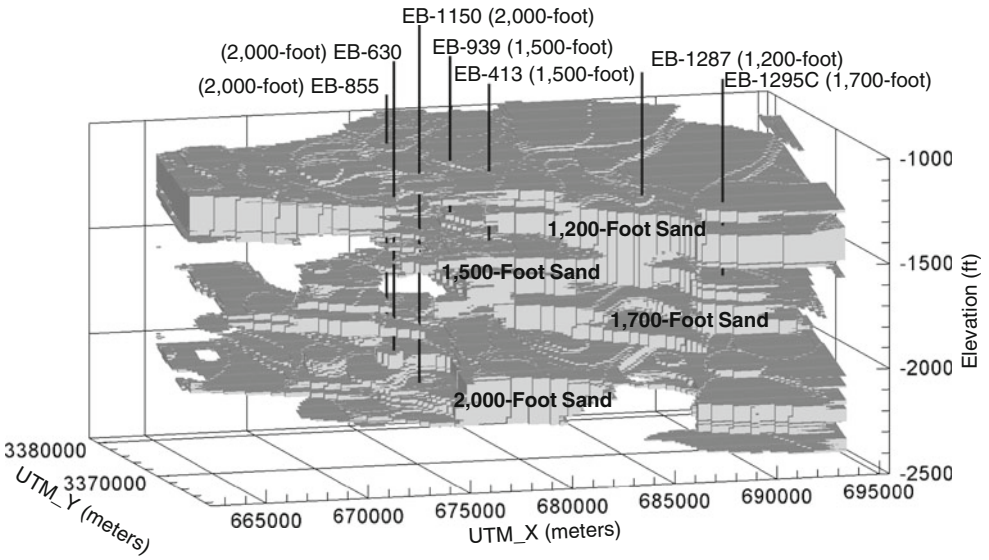

Fig. 6 Hydrostratigraphic architecture of the *1,200-foot* sand to the *2,000-foot* sand in the middle domain. The wells in the figure are public supply and industrial wells

 DOI 10.1007/s10040-013-1037-5

Leaky faults

The architecture of the Denham Springs-Scotlandville fault in Fig. 3 shows the role of the fault in controlling lateral hydraulic continuity. The conjoined areas of sand and clay units at the fault naturally create horizontal flow barriers. Potential horizontal flow pathways may be identified at the places where sands are conjoined at the fault. The results in Fig. 3 show a wide extent of horizontal flow pathways through the Denham Springs-Scotlandville fault to the 1,200-foot sand and the 2,000-foot sand in the middle domain. On the other hand, the 1,500-foot and 1,700-foot sands in the middle domain show fewer flow pathways for hydraulic connection through the Denham Springs-Scotlandville fault. Figures 4 and 5 show that there are a moderate number of horizontal flow pathways to the 1,200-foot sand and very limited horizontal flow pathways to the 2,000-foot sand in the middle domain through the Baton Rouge fault. However, the horizontal flow pathways through the Baton Rouge fault to the 1,500-foot sand and the 1,700-foot in the middle domain sand are extensive.

The actual fault permeability for the flow pathways depends on the clay content in the fault zone (Bense and Person 2006), which directly impacts on groundwater head across the fault. The USGS groundwater data suggested that the Baton Rouge fault is laterally a low-permeability fault zone as reflected by significant head differences across the fault (Meyer and Rollo 1965; Rollo 1969). The groundwater modeling results confirmed a low fault permeability for the Baton Rouge fault at the 2,000-foot sand (Torak and Whiteman 1982) and at the 1,500-foot sand (Tsai and Li 2008; Tsai 2010). The literature shows that the Denham Springs-Scotlandville fault has not been well studied. The current groundwater levels (EB-168 and EB-652) from the USGS database do not suggest significant hydraulic discontinuities across the Denham Springs-Scotlandville fault for the 1,500-foot sand.

Both faults are leaky faults. The flow pathways of the Denham Springs-Scotlandville fault allow groundwater to flow into the middle domain, which is heavily pumped. The flow pathways of the Baton Rouge fault allows saltwater intrusion into several freshwater sands (Tomaszewski 1996; Lovelace 2007, 2009; Anderson 2012)

Quantification of structural geology parameters

Figure 6 shows the simulated aquifer architecture from the 1,200-foot sand to the 2,000-foot sand in the middle domain based on the GP method. The 1,200-foot sand connects vertically to the 1,500-foot sand. The 2,000-foot sand is clearly separated from the 1,700-foot sand by a confining layer. There are four sand units between the 1,200-foot sand and the 2,000-foot sand, which are generally classified as the 1,500-foot sand and the 1,700-foot sand (Griffith 2003). Unlike the distinguishable 1,200-foot sand and the 2,000-foot sand, the separation of the 1,500-foot sand from the 1,700-foot sand is not well defined in the published cross sections (Rollo 1969; Griffith 2003). The findings of this study also show that they are not clearly separable. Therefore, in this study the 1,500-foot sand and the 1,700-foot sand are together treated as a single unit.

This section presents a regression technique and a clustering technique to quantify sand proportion, formation dip and sand unit offset on the faults. The main purpose of the regression technique is to determine the dip of a sand unit. Each sand unit shown in Fig. 7 is first visually distinguished. Given an east–west cross section, the top, middle and bottom elevations of sand units for the cross section are averaged. Repeating it for different east–west cross sections along the dip direction, the elevation points for the sands are obtained as shown in Fig. 8. Then, linear regression method weighted by the sample size is

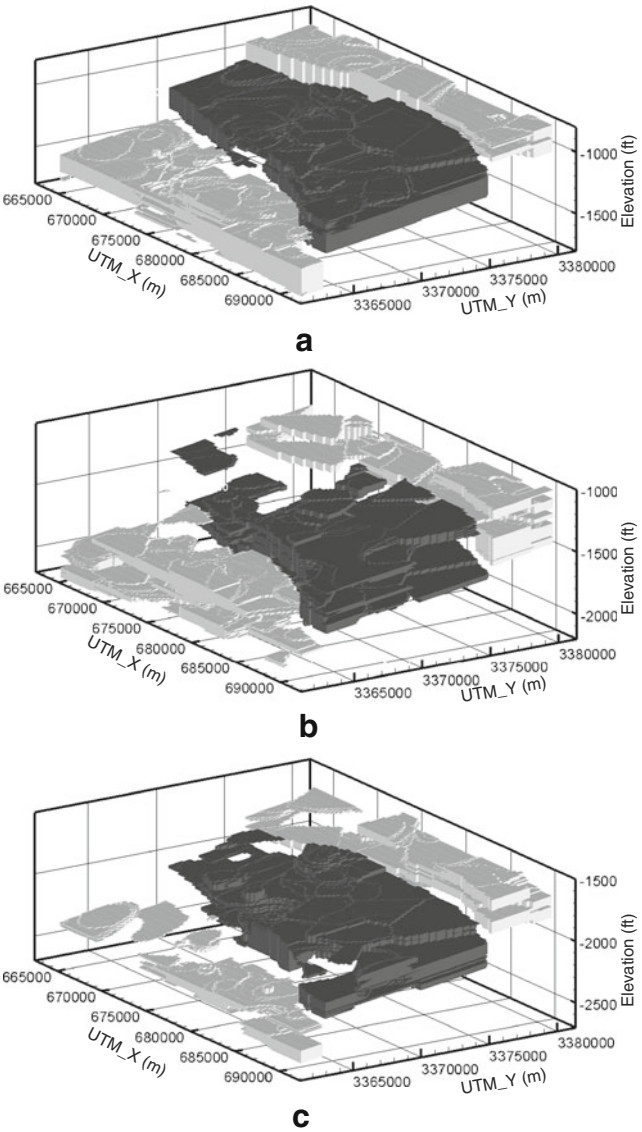

Fig. 7 Sand units and displacements on the faults for **a** the *1,200-foot* sad **b** the *1,500–1,700-foot* sands, and **c** the *2,000-foot* sand

DOI 10.1007/s10040-013-1037-5

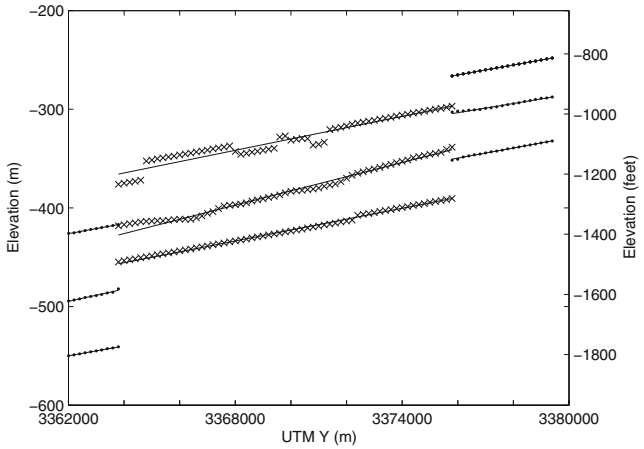

Fig. 8 Top, middle and bottom elevations of the 1,200-foot sand using the regression method

used to fit straight lines to the top, middle and bottom elevation points; and therefore, the dip is determined by the slope. Based on Fig. 8, the displacements of a sand unit on the faults can be calculated by the line dislocation. Moreover, based on Fig. 7 the proportion of sand in each domain can be calculated.

The clustering method is the second technique that is used to quantify the same geological structure parameters. Chamberlain (2012) determines the proportions of sand in clay with depth in a series of strike sections perpendicular to dip to identify sand-dominated zones in a sequence with a high degree of lateral stratigraphic variation. A similar approach is used to calculate the sand proportion with depth in a east–west direction using 200-foot (61 m) wide stripes immediately north and south of the faults. The variation in the proportion of sand with depth north and south adjacent to the Baton Rouge fault and the Denham Springs-Scotlandville Fault is determined as shown in Fig. 9.

The k-means clustering method (Lloyd 1982) is used to analyze Fig. 9 and determine the cluster centers and boundaries. The decision variable is the cluster elevation. The k-means automatically designates different clusters representing different aquifer units. The k-means provides the first moment of each cluster, which represents the mean elevation of a slice at a distance of 200 feet (60.96 m) along the fault and the mean sand ratio of this cluster. Since the number of clusters needs to be predefined for k-means method, several numbers of clusters were tested. It was found that using four clusters provides an excellent solution in terms of being able to accurately delineate the bottom elevation of the four aquifer units for the considered slice. This can be verified for example by comparing the cluster elevations in Fig. 9 (middle-south) to the aquifer units elevations in Fig. 6. The four clusters in the depth sequence represent the 1,200, 1,500, 1,700, and the 2,000-foot sand.

According to Fig. 9, the cluster centers and boundaries can be used to determine sand displacement on the faults and formation dip for the sands in the middle domain. Although the clustering method was able to identify the 1,500-foot sand and 1,700-foot sand as two separate sand units, they are represented as one unit with a mean value in order to compare the results with the regression method.

The calculated sand proportions of individual sands given the vertical intervals are shown in Table 3. Both methods show a high sand proportion for the 1,200-foot sand, which has more than 13 % of sand for the south and middle domain and has more than 16 % of sand in the north domain. The high sand proportion reflects the

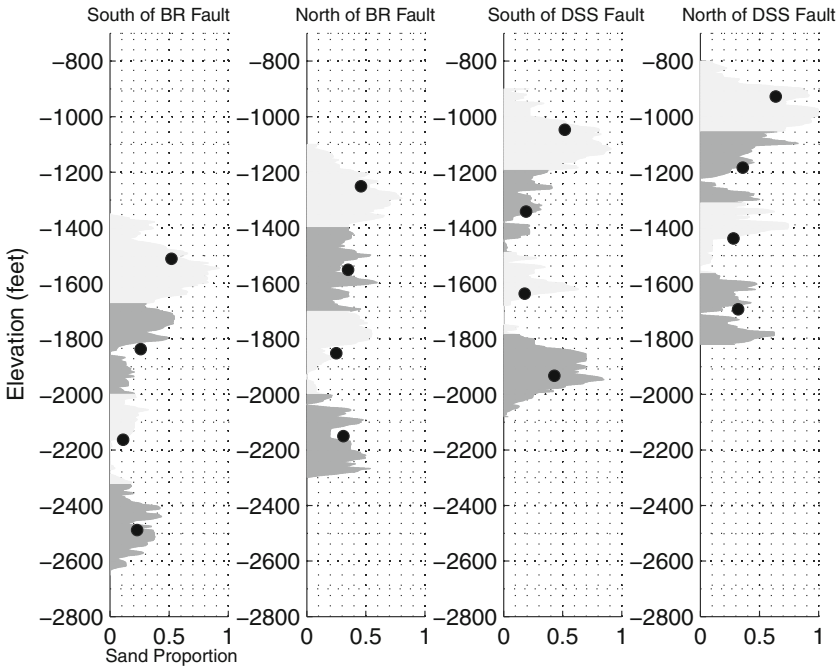

Fig. 9 Variation in the proportion of sand with depth immediately south and north of the Baton Rouge (BR) and Denham Springs-Scotlandville (DSS) faults using the clustering method. *Black dots* are centroids of the clusters

 DOI 10.1007/s10040-013-1037-5

Table 3 Estimated sand proportions

Sand	Regression method			Clustering method		
	South	Middle	North	South	Middle	North
1,200-foot sand	0.139	0.131	0.162	0.130	0.123	0.161
1,500–1,700-foot sands	0.112	0.122	0.128	0.094	0.122	0.161
2,000-foot sand	0.045	0.120	0.104	0.059	0.092	0.079
All sands	0.296	0.373	0.394	0.282	0.337	0.402

massive nature of the 1,200-foot sand, as shown in Fig. 7a. The 1,500–1,700-foot sands have more than 12 % of sand estimated by the regression method. However, the clustering method estimates a low sand proportion of 9.4 % for the south domain and high sand proportion 16.1 % for the north domain. Although most of the 1,500-foot sand in the industrial district and in West Baton Rouge Parish is missing as shown in Fig. 7b, which is potentially due to erosion as suggested by Chamberlain (2012), the sand proportion is similar to that of the 1,200-foot sand in the middle domain. This is because that significant proportion of the 1,500–1,700-foot sands extends over an extensive depth interval in East Baton Rouge Parish. The 2,000-foot sand has a low sand proportion of around 10 % for the middle domain and less than 8 % in the north and south domains due to a significant amount of sand missing in West Baton Rouge Parish, as shown in Fig. 7c. In summary, the total sand proportion in the south domain is less than 30 % and is more than 34 % in the middle domain and is around 40 % in the north domain. The calculated total sand proportion for the entire modeling area is 34 %, which is consistent with the total proportion of the sand indicators of the electric logs data 33.8 % and drillers' logs data 33.9 % for the considered range.

The calculated dips are shown in Table 4. The mean dip for the 1,200-foot sand and the 1,500-foot sand is 0.30°, and for the 2,000-foot sand is 0.38° using the regression method. The mean dips for the middle domain using the cluster method are similar for all sands, which vary from 0.33° to 0.35°. Moreover, the dip increases with depth (Griffith 2003). The average dip for all sand units is 0.33°, which is comparable to the dip 0.30° estimated from the cross sections in Griffith (2003) and 0.29° from the inverse solutions in Table 2.

The sand displacement on the faults is shown in Table 5. The clustering method estimates sand displacements on the Baton Rouge fault which increase from 262 ft (79.2 m) to 337 ft (102.7 m) for the 1,200-foot sand to the 2,000-foot sand, and are 20–30 ft (6.1 to 9.1 m) more than displacements calculated by the regression method. Durham and Peeples (1956) estimated a 344-ft (104.9 m) displacement on the Baton Rouge fault for the 2,000-foot sand, which is close to the result of the clustering method. Both methods have similar estimated sand displacements on the Denham Springs-Scotlandville fault for the 1,200-foot and the 1,500–1,700-foot sands, which are 120 ft (36.6 m) and 179 ft (54.6 m), respectively. The sand displacement on the 2,000-foot sand is estimated to be 239 ft (72.8 m) using the clustering method, which is 50 ft (15.2 m) more than the regression method. In summary, the sand displacement on the Baton Rouge fault is 100 ft (30.5 m) to 140 ft (42.7 m) more than that on the Denham Springs-Scotlandville fault. Also, the fault throw appears to increase with depth.

Interconnections between sand units

Since most of the industrial and public supply wells in Baton Rouge are screened in sand units in the middle domain, it is important to understand the interconnections between sand units in this domain. As shown in Fig. 10a, the 1,200-foot sand in the middle domain receives groundwater from the 1,200-foot sand and the 1,500–1,700-foot sands at the north due to the throw on the Denham Springs-Scotlandville fault. The flow pathways through the Denham Springs-Scotlandville fault are extensive according to Fig. 3. The 1,200-foot sand connects to the lower portion of the 1,000-foot sand and upper portion of the 1,200-foot sand south of the Baton Rouge fault, where the extent of flow pathways are moderate, as shown in Fig. 3. It is interesting to see the connection of the 1,200-foot sand to the 1,500-foot sand in the southeastern area of the middle domain, which indicates partial recharge to the 1,500-foot sand.

The 1,500-1,700-foot sands in the middle domain shown in Fig. 10b connect to the same sands unit north of the Denham Springs-Scotlandville fault. The extent of lateral flow pathways through the Denham Springs-Scotlandville fault are not significant as shown in Fig. 3, which indicates the importance of the 1,200-foot sand at the top to supply groundwater to these sands. The 1,500–1,700-foot sands extensively connect to the 1,200-foot

Table 4 Estimated formation dip (degrees) for sand units

Sand	Regression method			Clustering method
	South	Middle	North	Middle
1,200-foot sand	0.28±0.03	0.32±0.01	0.29±0.03	0.33±0.05
1,500–1,700-foot sands	0.28±0.02	0.32±0.03	0.31±0.03	0.34±0.05
2,000-foot sand	0.41±0.22	0.38±0.06	0.34±0.14	0.35±0.06

 DOI 10.1007/s10040-013-1037-5

Table 5 Estimated sand unit displacements in feet (and the parenthetical numbers are in meters) on the Baton Rouge (*BR*) fault and the Denham Springs-Scotlandville (*DSS*) fault

Sand	Regression method		Clustering method	
	BR Fault	DSS Fault	BR Fault	DSS Fault
1,200-foot sand	241±62 (73.4±18.9)	114±54 (34.7±16.5)	262±12 (79.9±3.7)	120±20 (36.6±6.1)
1,500–1,700-foot sands	290±59 (88.4±18.0)	173±50 (52.7±15.2)	298±17 (90.8±5.2)	180±28 (54.9±8.5)
2,000-foot sand	307±38 (93.6±11.6)	187±57 (57.0±17.4)	337±14 (102.7±4.3)	239±20 (72.8±6.1)

sand and the 1,500-foot sand in the south as shown in Fig. 4 due to significant fault throw on the Baton Rouge fault.

The 2,000-foot sand in the middle domain shown in Fig. 10c connects to the same sand and upper portion of the 2,400-foot sand north of the Denham Springs-Scotlandville fault. The connections are significant as shown in Fig. 3 due to significant fault throw. The 2,000-foot sand has a very limited connection to the lower portion of the 1,700-foot sand south of the Baton Rouge fault. As shown in the following discussion, the limited pathways still create enough avenues for saltwater into the 2,000-foot sand.

Baton Rouge aquifer-fault connections for saltwater intrusion

The vulnerability of the aquifer system to saltwater intrusion is assessed by mapping the potential flow pathways across the Baton Rouge fault with respect to the locations of municipal and industrial wells in the 1,200, the 1,500 and the 2,000-foot sand, which are currently under the threat of saltwater encroachment (Lovelace 2007). Using 2D cross sections that are based on the 3D hydrostratigraphic model is adequate for showing that the pumping wells are connected to the source of the saline water south of the Baton Rouge fault. Figure 11 shows the merger of the 1,200-foot sand and the 1,500-foot sand, which Fig. 6 depicts in three dimensions. The two sand units connect to the 1,200-foot sand south of the Baton Rouge fault. Three public supply wells are active along this cross section. There is no report of saltwater encroachment within the area of this cross section.

Figure 12 shows a sand connection from the 1,200-foot sand south of the fault to municipal wells EB-413 and EB-939 screened in the 1,500-foot sand. High chloride concentrations have been observed at observation well EB-917. The flow pathway is consistent with the results of saltwater intrusion modeling for the 1,500-foot sand (Tsai 2010). The identified leaky area also explains the salinity distribution in the depth around 1,500 feet below land surface documented by Anderson (2012), where relatively low chloride concentrations are observed at the south of the leaky area. Prior to development, the leaky area used to act as a natural outlet to discharge fresh groundwater to the south of the Baton Rouge fault. The groundwater level data in the 1930s from the online USGS National Water Information System shows southward flow direction. Well EB-326 had a water level of 64 ft (19.51 m) above NGVD29 in October 1936 in the 1,200-foot sand south of the fault. The head data at EB-84, EB-89, EB-311, and EB-312 indicates a water level 75 ft (22.86 m) above NGVD29 in October 1936 in the 1,500-foot sand north of the fault. This difference in water levels confirms that during pre-development pumping groundwater level in the 1,500-foot sand north of the fault was higher than that in the 1,200-foot sand south of the fault. However, heavy pumping in the 1,500-foot sand at Lula station and

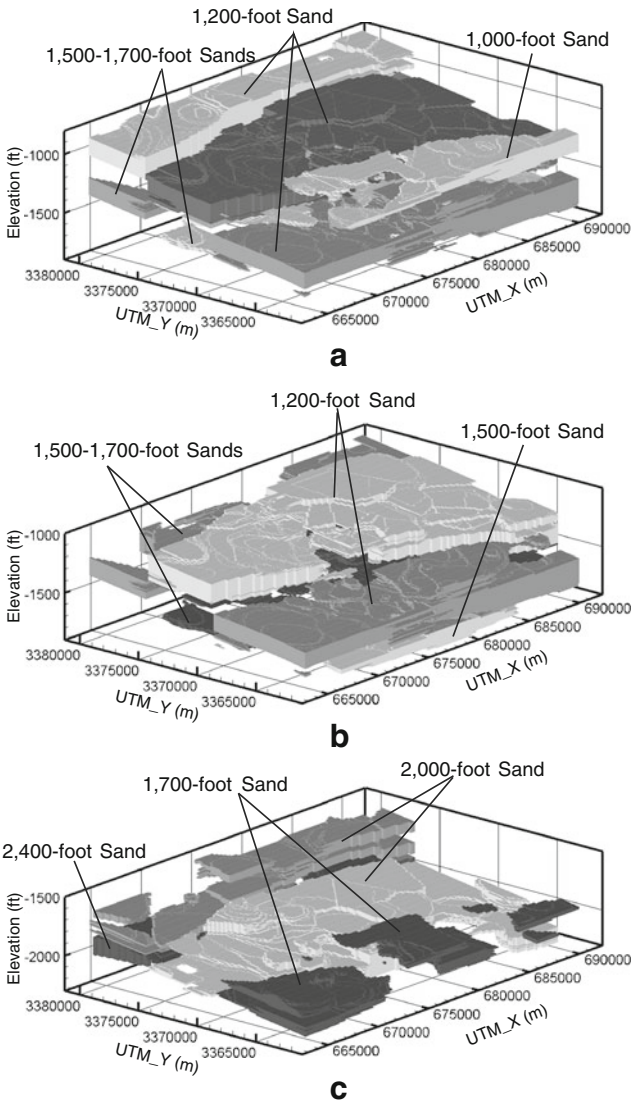

Fig. 10 Interconnections of sand units to the sand units in middle domain for **a** the *1,200-foot* sand, **b** the *1,500–1,700-foot* sands, and **c** the *2,000-foot* sand

DOI 10.1007/s10040-013-1037-5

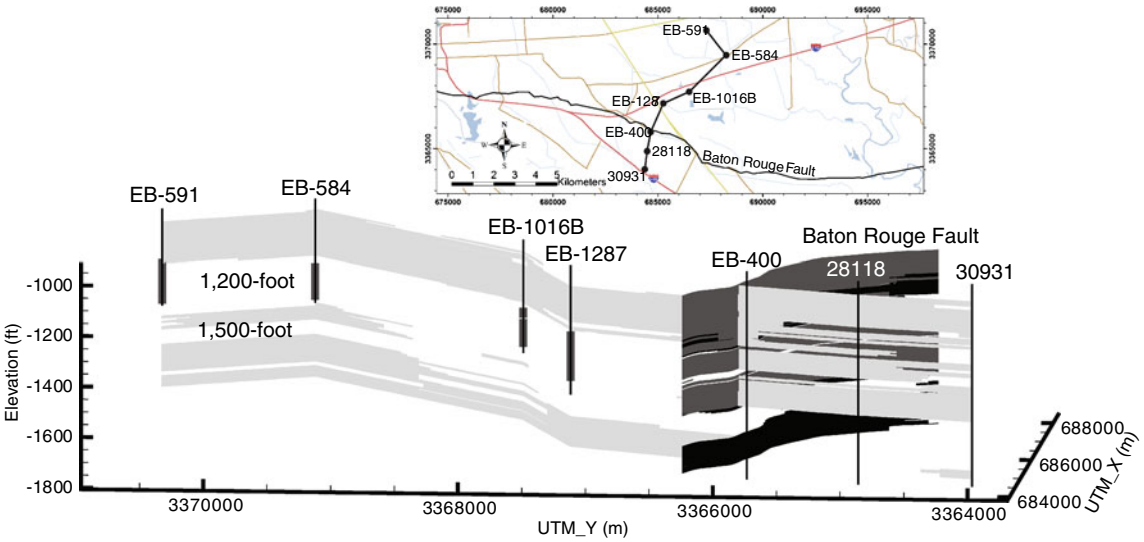

Fig. 11 A cross section shows the merger of the *1,200-foot* sand and the *1,500-foot* sand and their connection to the 1,200-foot sand south of the *Baton Rouge fault*. Sand units are transparent. *EB-1287*, *EB-1016B*, and *EB-584* are public supply wells. The *color lines* and areas in the inset map are defined in Fig. 1

Government Street station reversed the flow gradient causing brackish water to flow northward into the 1,500-foot sand (Morgan and Winner 1964; Meyer and Rollo 1965; Rollo 1969; Tomaszewski 1996).

Two leaky areas connected to the 2,000-foot sand through the Baton Rouge fault are identified in Fig. 4. Figure 13a shows a saltwater intrusion path starting in East Baton Rouge Parish to production well EB-1150 (Lovelace 2009). Figure 13b shows the detailed cross section that illustrates a potential saltwater intrusion path in West Baton Rouge Parish to production wells EB-630 and EB-1263. Again, these two pathways explain the spatial variations in salinity at a depth around 2,000 feet below land surface documented by Anderson (2012), where low groundwater salinities are found at the south of the leaky areas. For details on saltwater concentrations, the interested reader can compare the main flow pathways in the 1,500-foot sand in the middle, and the east and west flow pathways in the 2,000-foot sand with the saltwater concentration maps of Anderson (2012, Figure 4.9 C,D). Since these two studies were conducted independently, it is important to note that the potential pathways that are identified from the results of this study coincide spatially with leaky areas of high salinities along the fault. This

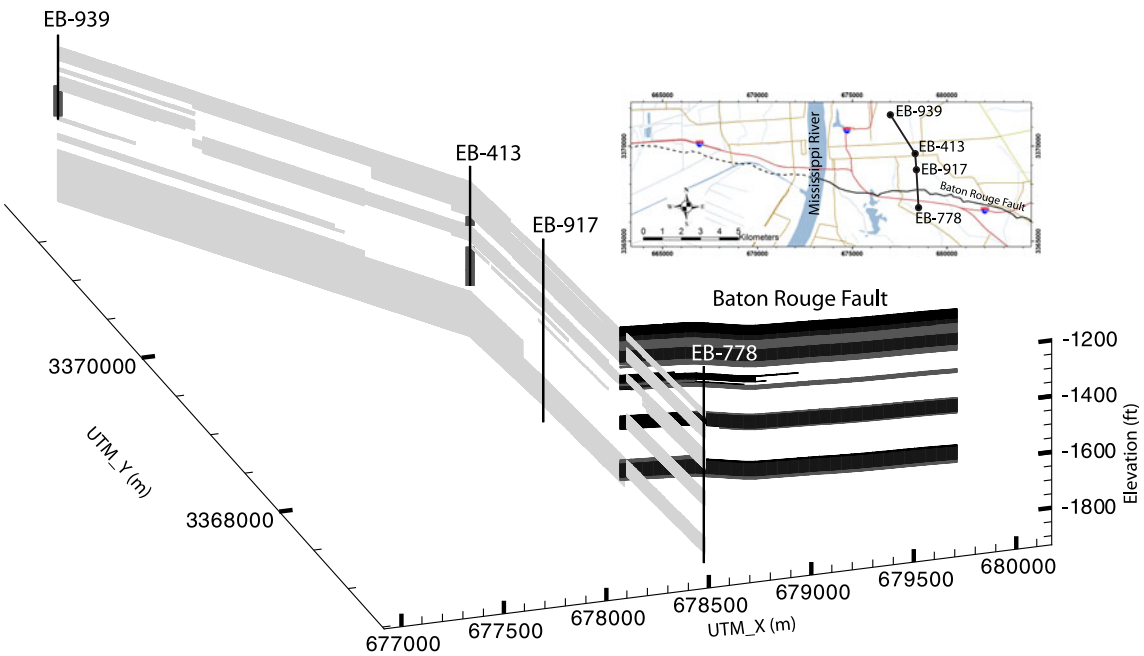

Fig. 12 A cross section shows the connection of the 1,500–1,700-foot sands to the 1,200- foot sand south of the Baton Rouge fault. Sand units are transparent. *EB-413* in the Government Street station and *EB-939* in the Lula station are public supply wells. The *color lines* and areas in the inset map are defined in Fig. 1

 DOI 10.1007/s10040-013-1037-5

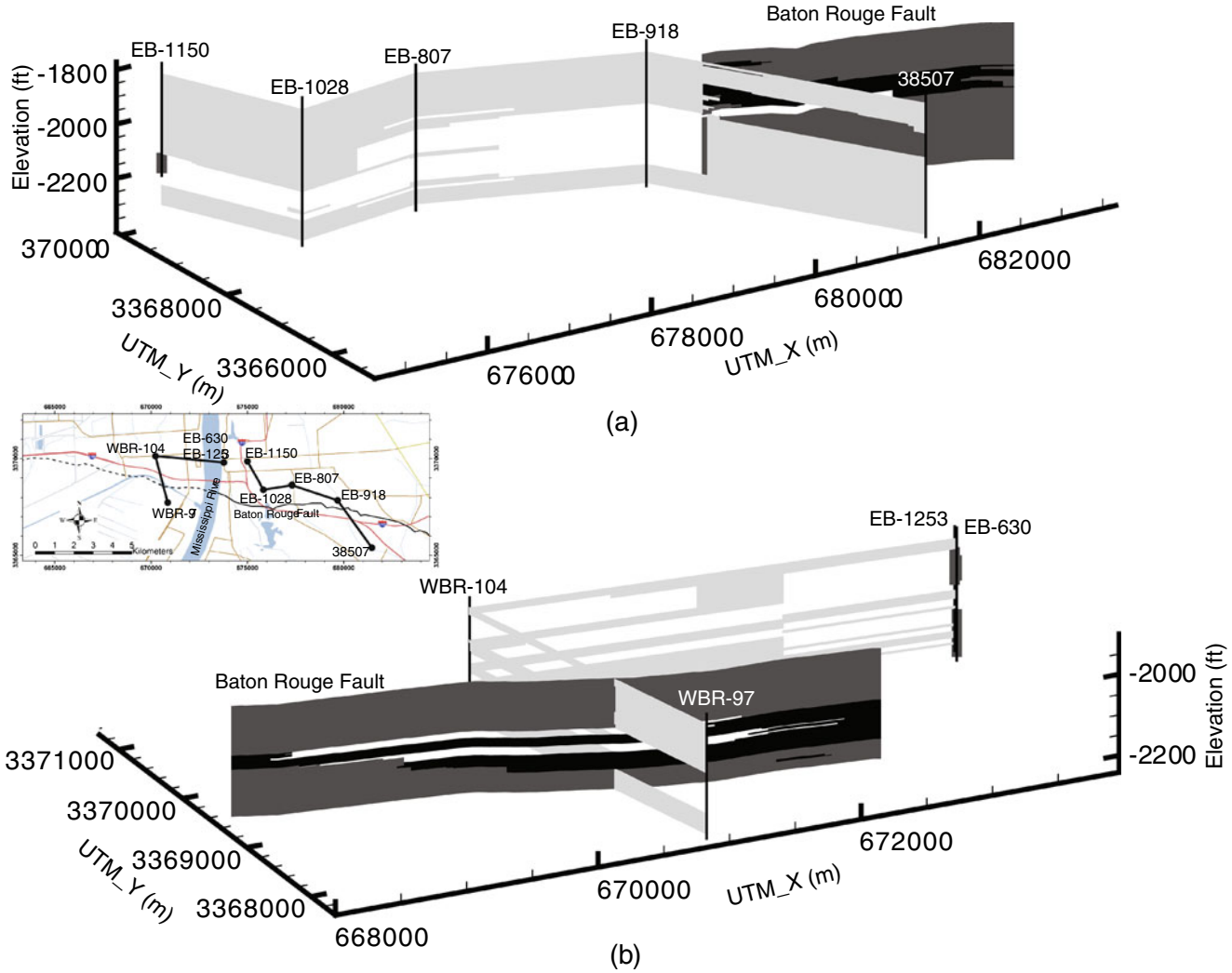

Fig. 13 Two cross sections show the connections of the 2,000-foot sand to the 1,700-foot sand south of the Baton Rouge fault in (a) East Baton Rouge Parish and (b) West Baton Rouge Parish. Sand units are transparent. *EB-1150*, *EB-1253*, and *EB-630* are public supply wells. The *color lines* and areas in the inset map are defined in Fig. 1

also suggests that fresh groundwater flowed southward from the 2,000-foot sand north of the Baton Rouge fault into the 1,700-foot sand south of the Baton Rouge fault prior to heavy pumping. Current high groundwater withdrawals from the 2,000-foot sand by the water company and the industries have reversed the flow direction and have caused saltwater intrusion into the 2,000-foot sand (Lovelace 2007).

Conclusions

The generalized parameterization (GP) method is shown to be an effective indicator geostatistical method for reconstructing hydrostratigraphic architecture of a complex fluvial binary siliciclastic aquifer system. By depicting the spatial extent of sand units, the derived geological architecture shows interconnections among different sand units, flow pathways across faults, and connections of production wells to the potential leaky areas of the Baton Rouge fault. The regression method and the clustering method are effective methods for post-analyzing important geological parameters such as formation dip, sand proportion, and sand unit displacement on the fault.

The study finds strong hydraulic connection between the 1,200 and the 1,500-foot sand. Merger of the sand units indicates groundwater recharge from the 1,200-foot sand to the 1,500-foot sand. However, there is a distinct clay confining layer to separate the 2,000-foot sand from the 1,700-foot sand. The hydrostratigraphy also reveals four sand deposits that compose the 1,500-foot sand and the 1,700-foot sand. In general, sand deposition is not uniform, due to spatial and temporal variations in fluvial processes (Chamberlain 2012). The study shows that there is large amount of missing sand in 1,500-foot sand in the industrial district and in West Baton Rouge Parish, which is possibly due to the presence of an erosional unconformity (Chamberlain 2012).

The sand unit displacement on the Baton Rouge fault and the Denham Springs-Scotlandville fault is significant. The Baton Rouge fault has higher sand displacement than

 DOI 10.1007/s10040-013-1037-5

the Denham Springs-Scotlandville fault. Displacement increases over depth. Due to non-uniform fault throw and sand deposition, the study reveals non-uniform flow pathways that connect different sand units at the fault planes. In particular, the identified flow pathways through the Baton Rouge fault provide important information for understanding patterns of salinization of freshwater aquifers in the East Baton Rouge Parish.

Establishing the detailed 3D fault-aquifer sedimentary architecture of the Baton Rouge aquifer system is a prerequisite to future work on saltwater intrusion in the study area. The detailed fault-aquifer architecture provides information about connections between the aquifer units, which have significant implications on the salt-water intrusion problem. For example, the simulation of the salt-water intrusion in 1,200 and 1,500-1,700-foot sand should not be done separately, since they are very well connected in the middle zone. On the other hand, the industrial aquifer unit 2,000-foot sand is not connected to any of the units above. More importantly, the identified flow pathways through the Baton Rouge fault are prerequisites for modeling salt-water intrusion from the south to the north of the Baton Rouge fault. For example, without the fine discretization that this sedimentary architecture model provides, especially in the vertical direction, the narrow connection in the 2,000-foot sand in East Baton Rouge Parish that allows major leakage from the south would have been missed. Finally, by accounting for the geometry and locations of the flow pathways across the faults and the interconnections of different aquifer units, the sedimentary architecture makes the geological structure of the salt-water intrusion model consistent with the real geology of the aquifer. These shall improve the salt-water intrusion model adequacy.

Acknowledgements This study was supported in part by the National Science Foundation under Grant No. 1045064 and Grant/Cooperative Agreement Number G10AP00136 from the United States Geological Survey (USGS). Its contents are solely the responsibility of the authors and do not necessarily represent the official views of the USGS. The authors acknowledge Liangping Li, Gary Weissmann and two anonymous reviewers for providing constructive comments which improved the manuscript.

References

Anderson CE (2012) Sources of Salinization of the Baton Rouge Aquifer System: southeastern Louisiana. MSc Thesis, Louisiana State University, USA, 75 pp

Bense VF, Person MA (2006) Faults as conduit-barrier systems to fluid flow in siliciclastic sedimentary aquifers. Water Resour Res 42:18

Bersezio R, Giudici M, Mele M (2007) Combining sedimentological and geophysical data for high-resolution 3-D mapping of fluvial architectural elements in the Quaternary Po plain (Italy). Sediment Geol 202:230–248

Bredehoeft JD (1997) Fault permeability near Yucca Mountain. Water Resour Res 33:2459–2463

Buono A (1983) The Southern Hills regional aquifer system of southeastern Louisiana and southwestern Mississippi. US Geol Surv Water Resour Invest Rep 83-4189

Caers J (2001) Geostatistical reservoir modelling using statistical pattern recognition. J Pet Sci Eng 29:177–188

Chamberlain EL (2012) Depositional Environments of Upper Miocene through Pleistocene Siliciclastic Sediments, Baton Rouge Aquifer System, southeastern Louisiana. MSc Thesis, Louisiana State University, USA, 66 pp

Chen JS, Rubin YR (2003) An effective Bayesian model for lithofacies estimation using geophysical data. Water Resour Res 39:11

Chester FM, Evans JP, Biegel RL (1993) Internal structure and weakening mechanism of the San-Andreas fault. J Geophys Res-Solid Earth 98:771–786

Chilès JP, Delfiner P (1999) Geostatistics: modeling spatial uncertainty. Wiley, New York, 734 pp

Comunian A, Renard P, Straubhaar J, Bayer P (2011) Three-dimensional high resolution fluvio-glacial aquifer analog, part 2: geostatistical modeling. J Hydrol 405:10–23

Desbarats AJ, Bachu S (1994) Geostatistical analysis of the aquifer heterogeneity from the core scale to the basin scale: a case study. Water Resour Res 30:673–684

Durham CO, Peeples FM (1956) Pleistocene fault zone in southeastern Louisiana. Trans Gulf Coast Assoc Geol Soc 6:65–66

Engdahl NB, Weissmann GS, Bonal ND (2010) An integrated approach to shallow aquifer characterization: combining geophysics and geostatistics. Comput Geosci 14:217–229

Ezzedine S, Rubin Y, Chen JS (1999) Bayesian method for hydrogeological site characterization using borehole and geophysical survey data: theory and application to the Lawrence Livermore National Laboratory Superfund site. Water Resour Res 35:2671–2683

Fairley J, Heffner J, Hinds J (2003) Geostatistical evaluation of permeability in an active fault zone. Geophys Res Lett 30(18):1962

Falivene O, Cabrera L, Saez A (2007) Large to intermediate-scale aquifer heterogeneity in fine-grain dominated alluvial fans (Cenozoic As Pontes Basin, northwestern Spain): insight based on three-dimensional geostatistical reconstruction. Hydrogeol J 15:861–876

Faunt CC, Belitz K, Hanson RT (2010) Development of a three-dimensional model of sedimentary texture in valley-fill deposits of Central Valley, California, USA. Hydrogeol J 18:625–649

Griffith JM (2003) Hydrogeologic framework of southeastern Louisiana. Water resources technical report 72, Louisiana Department of Transportation and Development, Baton Rouge, LA

Hanor J, Chamberlain EL, Tsai FT (2011) Evolution of the Permeability Architecture of the Baton Rouge Fault Zone, Louisiana Gulf Coastal Plain. American Geophysical Union Fall Meeting, San Francisco, December 5–9, 2011

Hansen N (2006) The CMA evolution strategy: a comparing review. In: Lozano JA, Larrañga P, Inza I, Bengoetxea E (eds) Towards a new evolutionary computation: advances in estimation of distribution algorithms. Springer, Berlin, pp 75–102

Hansen N, Muller SD, Koumoutsakos P (2003) Reducing the time complexity of the derandomized evolution strategy with covariance matrix adaptation (CMA-ES). Evol Comput 11:1–18

Hooke R, Jeeves TA (1961) Direct search solution of numerical and statistical problems. J ACM 8 (2):212–229

Johnson NM (1995) Characterization of alluvial hydrostratigraphy with indicator semivariograms. Water Resour Res 31:3217–3227

Johnson NM, Dreiss SJ (1989) Hydrostratigraphic interpretation using indicator geostatistics. Water Resour Res 25:2501–2510

Journel AG (1983) Nonparametric-estimation of spatial distributions. J Int Assoc Math Geol 15:445–468

Koltermann CE, Gorelick SM (1996) Heterogeneity in sedimentary deposits: a review of structure-imitating, process-imitating, and descriptive approaches. Water Resour Res 32:2617–2658

Li L, Zhou H, Hendricks Franssen HJ, Gómez-Hernández JJ (2012a) Groundwater flow inverse modeling in non-multiGaussian media: performance assessment of the normal-score Ensemble Kalman Filter. Hydrol Earth Syst Sci 16:573–590. doi:10.5194/hess-16-573-2012

Li L, Zhou H, Hendricks Franssen HJ, Gómez-Hernández JJ (2012b) Jointly mapping hydraulic conductivity and porosity by assimilating concentration data via Ensemble Kalman Filter. J Hydrol 428–429:152–169. doi:10.1016/j.jhydrol.2012.01.037

Linde N, Binley A, Tryggvason A, Pedersen LB, Revil A (2006) Improved hydrogeophysical characterization using joint inversion of cross-hole electrical resistance and ground-penetrating radar traveltime data. Water Resour Res 42:16

Lloyd SP (1982) Least-squares quantization in PCM. IEEE Trans Inf Theory 28:129–137

Lovelace JK (2007) Chloride Concentrations in ground water in East and West Baton Rouge parishes, Louisiana. US Geol Surv Sci Invest Rep 2004-05

Lovelace JK (2009) Ground water levels and salt water encroachment in major aquifers in Louisiana. USGS Ground Water Summit, February 4, 2009, USEPA, Dallas, TX

McCulloh RP, Heinrich PV (2012) Surface faults of the South Louisiana Growth-Fault Province. In: Cox, RT, Tuttle M, Boyd O, Locat J (eds) Recent advances in North American paleoseismology and neotectonics east of the Rockies and use of the data in risk assessment and policy. Geological Society of America, Boulder, CO

Meyer RR, Rollo JR (1965) Saltwater encroachment, Baton Rouge area. Louisiana Department of Conservation, Louisiana Geological Survey and Louisiana Department of Public Works Water Resources, Baton Rouge, LA, 9 pp

Meyer RR, Turcan AN, Jr (1955) Geology and ground-water resources of the Baton Rouge area, Louisiana. US Geol Surv Water Suppl Pap 1296, 138 pp

Miller RB, Castle JW, Temples TJ (2000) Deterministic and stochastic modeling of aquifer stratigraphy, South Carolina. Ground Water 38:284–295

Morgan CO, Winner MD, Jr (1964) Salt-water encroachment in aquifers of the Baton Rouge area: preliminary report and proposal. Louisiana Department of Public Works, Baton Rouge, LA, 37 pp

Nishikawa T, Siade AJ, Reichard EG, Ponti DJ, Canales AG, Johnson TA (2009) Stratigraphic controls on seawater intrusion and implications for groundwater management, Dominguez Gap area of Los Angeles, CA, USA. Hydrogeol J 17:1699–1725

Proce CJ, Ritzi RW, Dominic DF, Dai ZX (2004) Modeling multiscale heterogeneity and aquifer interconnectivity. Ground Water 42:658–670

Rollo JR (1969) Salt-water encroachment in aquifers of the Baton Rouge area, Louisiana. Louisiana Department of Conservation, Louisiana Geological Survey, and Louisiana Department of Public Works, Baton Rouge, LA, 45 pp plus plates

Rubin Y (2003) Applied stochastic hydrogeology. Oxford University Press, New York, 391 pp

Salve R, Oldenburg CM (2001) Water flow within a fault in altered nonwelded tuff. Water Resour Res 37:3043–3056

Sargent BP (2012) Water use in Louisiana, 2010. Special report no. 17 (revised), Louisiana Department of Transportation and Development Water Resources, Baton Rouge, LA, 135 pp

Scharling PB, Rasmussen ES, Sonnenborg TO, Engesgaard P, Hinsby K (2009) Three-dimensional regional-scale hydrostratigraphic modeling based on sequence stratigraphic methods: a case study of the Miocene succession in Denmark. Hydrogeol J 17:1913–1933

Schulmeister MK, Butler JJ, Healey JM, Zheng L, Wysocki DA, McCall GW (2003) Direct-push electrical conductivity logging for high-resolution hydrostratigraphic characterization. Ground Water Monit Remediat 23:52–62

Sibson R (1980) Vector identity for Dirichlet tessellation. Math Proc Camb Philos Soc 87:151–155

Strebelle S (2002) Conditional simulation of complex geological structures using multiple-point statistics. Math Geol 34:1–21

Tartakovsky AM, Bolster D, Tartakovsky DM (2008) Hydrogeophysical approach for identification of layered structures of the vadose zone from electrical resistivity data. Vadose Zone J 7:1207–1214

Tomaszewski DJ (1996) Distribution and movement of saltwater in aquifers in the Baton Rouge area, Louisiana, 1990–92, Technical Report, Louisiana Department of Transportation and Development Water Resources, Baton Rouge, LA

Torak LJ, Whiteman CD Jr (1982) Applications of Digital Modeling for Evaluating the Ground-water Resources of the "2,000-Foot" Sand of the Baton Rouge Area, Louisiana. Water Resources Technical Report no. 27, Louisiana Department of Transportation and Development, Office of Public Works, Baton Rouge, LA, 87 pp

Trevisani S, Fabbri P (2010) Geostatistical modeling of a heterogeneous site bordering the Venice Lagoon, Italy. Ground Water 48:614–623

Tsai FTC (2006) Enhancing random heterogeneity representation by mixing the kriging method with the zonation structure. Water Resour Res 42:W08428

Tsai FTC (2009) Indicator generalized parameterization for interpolation point selection in groundwater inverse modeling. ASCE J Hydrol Eng 14(3):233-242

Tsai FTC (2010) Bayesian model averaging assessment on groundwater management under model structure uncertainty. Stoch Env Res Risk A 24:845–861

Tsai FTC, Yeh WWG (2004) Characterization and identification of aquifer heterogeneity with generalized parameterization and Bayesian estimation. Water Resour Res 40:W10102

Tsai FTC, Li X (2008) Inverse groundwater modeling for hydraulic conductivity estimation using Bayesian model averaging and variance window. Water Resour Res 44(9):W09434. doi:10.1029/2007WR006576

Weissmann GS, Carle SF, Fogg GE (1999) Three dimensional hydrofacies modeling based on soil surveys and transition probability geostatistics. Water Resour Res 35:1761–1770

Weissmann GS, Fogg GE (1999) Multi-scale alluvial fan heterogeneity modeled with transition probability geostatistics in a sequence stratigraphic framework. J Hydrol 226:48–65

Wiederhold H, Rumpel HM, Auken E, Siemon B, Scheer W, Kirsch R (2008) Geophysical methods for investigation and characterization of groundwater resources in buried valleys. Grundwasser 13:68–77

Zappa G, Bersezio R, Felletti F, Giudici M (2006) Modeling heterogeneity of gravel-sand, braided stream, alluvial aquifers at the facies scale. J Hydrol 325:134–153

Zhou H, Li L, Hendricks Franssen HJ, Gómez-Hernández JJ (2012) Pattern recognition in a bimodal aquifer by normal score Ensemble Kalman Filter. Math Geosci. doi:10.1007/s11004-011-9372-3